Nanoscale Advances

PAPER

View Article Online
View Journal | View Issue

Cite this: *Nanoscale Adv.*, 2019, **1**, 1249

Transparent superhydrophilic and superhydrophobic nanoparticle textured coatings: comparative study of anti-soiling performance†‡

Gyoung Gug Jang, *[a] D. Barton Smith,[a] Georgios Polizos,[a] Liam Collins,[b] Jong K. Keum[b] and Dominic F. Lee[c]

The anti-soiling (AS) performance of highly reflective, superhydrophilic (SPH, 0° water contact angle) coated mirrors was characterized and compared with that of superhydrophobic (SP, >165° water contact angle) coated mirrors. A simple one-step nanotextured silica nanoparticle coating on a mirror exhibited SPH properties associated with hydrophilic rough surfaces. Another mirror surface post-functionalized with low-surface-energy ligand molecules displayed SP behavior. Both coated mirrors, with no solar reflectance loss, demonstrated excellent AS performance because the engineered surface roughness reduced the adhesive force of dust particles. The daily degradation in solar reflectance induced by dust accumulation under outdoor field testing demonstrated that the SPH- and SP-coated mirrors, compared with an uncoated mirror, maintained higher solar reflectance, which was associated with the designed self-cleaning behavior and natural cleaning. However, over the long term, dust-moisture cementation—evidenced by organic hard water stains on the mirror—initiated unrecoverable reflectance loss on the SP-coated mirror after 3 months, whereas the SPH-coated mirror maintained higher reflectance for 7.5 months. Considering fabrication costs and maintenance, SPH-coated nanotextured mirrors offer potential benefits for application in solar energy harvesting.

Received 13th November 2018
Accepted 20th December 2018

DOI: 10.1039/c8na00349a

rsc.li/nanoscale-advances

1. Introduction

Surface engineering of an anti-soiling (AS) feature on the reflective surfaces of solar energy devices is important for stable solar energy harvesting, because accumulating dust layers induce significant scattering and absorption of incident solar irradiation.[1–9] For example, concentrated solar power (CSP) technologies generate power by using mirrors to reflect and concentrate a large area of sunlight onto a small area of a receiver.[1,7,10–14] Maintaining clean mirror surfaces is important because CSP plants, mainly built in arid desert areas, experience severe dust accumulation. In efforts to mitigate soiling and maintain clean surfaces, many studies have explored natural soiling of reflective surfaces and environmentally friendly cleaning methods in the field.[1–3,5,8–14] Recent progress in nanotechnology (*e.g.*, transparent superhydrophobic [SP] coatings[6,15–22]) suggests a potential breakthrough in a unique surface self-cleaning technology that could significantly enhance the reliability and efficiency of solar panel glass and solar mirrors while drastically reducing cleaning and maintenance costs. A reduction in maintenance costs as a result of self-cleaning surfaces could have a significant impact on energy harvesting.

Self-cleaning coatings can be divided into two categories: hydrophobic and hydrophilic. Both types of coatings clean themselves through the action of water, the former by rolling water droplets off and the latter by forming water into a thin sliding layer that carries away dirt.[6,16,20] Recently, we reported that highly transparent SP nanoparticle (NP) -textured coatings exhibited excellent AS performance, which was associated with surface roughness at the scale of <100 nm and with a non-wetting property.[21,22] The rough surface structure of the SP NP coatings provided an intrinsic capability to repel small dust particles by reducing the adhesive force between dust particles and the coated surface. An SP-coated mirror maintained high reflectance by resisting dust accumulation during testing in an outdoor environment.[21] Also, the results indicated that the NP-textured coating before post-fluorination for SP performance

[a]*Energy and Transportation Science Division, Oak Ridge National Laboratory (ORNL), Oak Ridge, TN 37831, USA. E-mail: jangg@ornl.gov*

[b]*Center for Nanophase Materials Science, ORNL, USA*

[c]*Sustainable Electricity Program Office, ORNL, USA*

‡ Electronic supplementary information (ESI) available. See DOI: 10.1039/c8na00349a

was highly hydrophilic, with a measured water contact angle (WCA) of 0–5°. Based on the accepted definition of superhydrophilicity (*i.e.,* textured materials having a surface roughness factor of [$r > 1$], on which water spreads completely), NP-textured surfaces can be called superhydrophilic (SPH) materials.[23]

Inspired by the performance of the one-step SPH NP-textured coating with a significant reduction in adhesive force, in this study, we systematically compared the AS behaviour of an SPH coating with that of an SP coating to evaluate their feasibility for use on solar energy-harvesting mirrors under outdoor environments. Many studies predict that hydrophilic and hydrophobic surfaces have potential to benefit AS performance.[21,22,24] However, to our best knowledge, a rigorous comparative study of SP and SPH self-cleaning surfaces has not been reported. We found that the adhesive force of simulated dust particles on SPH surfaces was similar to the force on SP surfaces, because both have NP-textured surfaces that afford excellent AS performance against inorganic dust particles. Outdoor field tests demonstrated a significant reduction in dust accumulation and outstanding self-cleaning performance for an SPH-coated mirror compared with an SP-coated mirror and an uncoated mirror. Note that without the toxic and expensive post-fluorination step, the simple, environmentally friendly SPH textured coating outperformed the SP coating, according to the field testing.

2. Experimental section

2.1. Preparation of SiO_2 nanoparticle self-assembly coating

The NP coatings were deposited on solar mirrors by a drawdown coating method, as reported in our previous paper.[21] Briefly, the silica oxide NP coating solution (a mixture of Aerosol380® and silica sol–gel at a weight ratio of 2 : 1 in ethanol) was placed on the glass at the leading edge of the mirror, and a grooved rod (*i.e.*, RDS #3) spread the solution at a speed of 2.54 cm s^{-1} using a drawdown machine. The process left a uniform wet film (designed to be ~7.6 μm) that dried at room temperature. The hydroxyl groups on the mirror surface promoted uniform wetting of the surface with the hydrophilic SiO_2 NP solution. The silica sol–gel served as a binder between the NPs and the mirror surface [ESI‡]. After a few seconds, the wet film dried and left a uniformly thick, transparent thin film (200–250 nm thickness with two coating layers). The topography and surface functionality of the coatings on the solar mirrors were controlled by varying the sol–gel/NP weight ratio from 2 to 64. As the ratio increased, the WCA increased from 0° to 58°. After thermal vapor deposition of fluorosilane (*i.e.*, (heptadecafluoro-1,1,2,2-tetrahydrodecyl)trichlorosilane) at 120 °C, the WCAs of the coatings were converted to a range from 111° to 165°.

2.2. Characterization

Scanning electron microscopy (SEM) was carried out using a field emission scanning electron microanalyzer (Merlin, Carl Zeiss AG). WCAs were measured by an optical tensiometer (OneAttension, Biolin Scientific). Specular reflectances in a spectral band from 330 to 2500 nm were measured using a portable reflectometer (410-Solar, Surface Optics Corporation). The surface chemistry of a coated sample was characterized using X-ray photo-electron spectroscopy (XPS). Dust particle sizes were determined by optical microscopy. The soiling rate was measured using the apparatus developed in our previous work.[21] Standard test dust (ISO 12103-1 A4 Coarse Sand, 0.9–352 μm of particle size distribution) was used for the dust soiling. Using atomic force microscopy (AFM), we measured the adhesive force between a synthetic dust particle made of silica (15 μm diameter silica sphere attached to the end of the tip) and the NP-textured surfaces. The AFM used for the humidity study was a Cypher ES instrument (Asylum Research and Oxford Instr. Company), used in conjunction with a borosilicate colloid probe cantilever (Novascan) of 6 μm diameter and a calibrated spring constant of 3.58 N m^{-1}. For humidity control, the inlet for the environmental scanner was supplied with a continuous flow of nitrogen, diverted from a homemade gas humidifier. The gas bubbler/humidifier could be controlled to determine the humidity passing to the cell, which was measured close to the microscope cell by a humidity probe. It was possible to control the humidity in a range of 2–80% relative humidity (RH). For each humidity measurement, the cell environment was allowed to stabilize for ~30 min before commencement of the adhesion measurement. For each RH level, a total of 256 force curves were collected in a grid over 30 μm of each sample. From these measurements, the mean and standard deviation adhesive forces were calculated and plotted *versus* humidity.

3. Results and discussion

3.1. Transparent SPH-coated mirrors

A transparent SiO_2 NP self-assembled thin layer was deposited by rod drawdown coating. The transparent SPH coatings on a solar mirror were fabricated as two drawdown coating layers with SiO_2 NPs and silicate sol–gel binder [Fig. 1a]. SEM images of the two-layer NP coatings show a uniformly textured thin layer with a 200–250 nm thickness [Fig. 1b and c]. The coating exhibited strong hydrophilicity, with complete spreading of water (0° WCA) due to hydroxyl groups on the rough surface. After thermal fluorosilane vapor deposition, the textured coating exhibited SP characteristics, having a >165° WCA compared with the ~45° WCA of an uncoated mirror. The surface morphology and thickness of the coating showed no distinguishable difference after fluorination. The surface chemical component of the XPS analysis showed high silicon and oxygen contents at the surface of the SPH coating compared with other elements, which was explained by the presence of the intrinsic SiO_2 NP layers [Table 1]. The SP-coated surface showed the existence of fluorine due to the fluorination process. Further XPS analysis is available in the ESI.‡

The NP-coated mirror exhibited good durability against the abrasive effect of falling sand (*e.g.,* simulation of 15 years of sand falling on the coating) and the aging effect of an accelerated ultraviolet light.[21] The added sol–gel (*i.e.,* acidic catalysed hydrolytic condensation of TEOS) acted as a strong binder,

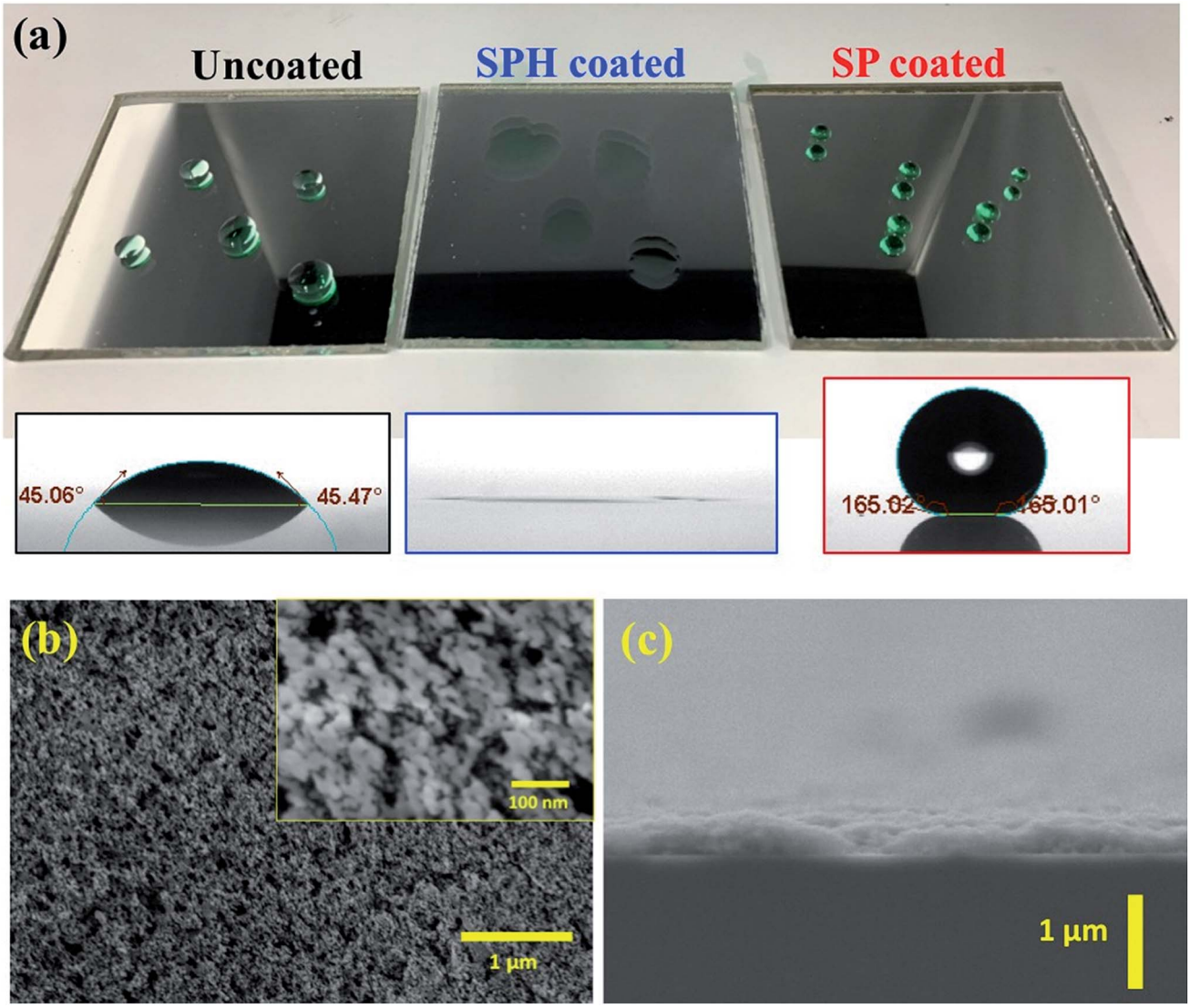

Fig. 1 (a) Highly reflective, anti-soiling nanoparticle-texture solar mirrors (7.6 × 7.6 cm^2) with no coating, superhydrophilic (SPH) coating, and superhydrophobic (SP) coating. Insets are water contact angle measurements on the coated mirrors (the measured water droplet volume = 5–10 μl). (b) SEM images of coated mirror surface, showing characteristics of SPH nanotexturing. (c) SEM cross-sectional view of SPH coating.

Table 1 Chemical composition of SP and SPH coating determined by XPS

	O–Si	O	Si–O	Si	C	C-Fx	F	O–Si/Si–O	C-Fx/F
Uncoated	53.7	6	27.1	0	7.2	0	0	2.0	—
SPH	53.1	**10.0**	27.1	**3.0**	6.3	0	0	2.0	—
SP	45.8	0.4	22.5	0.0	7.7	**7.0**	**15.5**	2.0	0.45

resulting in good mechanical stability that could be attributed to the noncovalent bonding (*e.g.,* hydrogen bonding with hydroxyl groups *via* hydrolytic condensation) formed between the NP, binder, and glass surface.[25,26] The SPH textured coating was studied for characterization and AS performance compared with the SP coating.

The SiO_2-NP-based drawdown coating exhibited excellent uniform optical properties on a large scale.[21] Fig. 2 shows the average specular reflectances at seven wavelength bands extending from 335 to 2500 nm on the SPH-coated and uncoated mirrors at a single measurement location for each mirror. The spectrum bands of the SPH coating had a slightly higher reflectance than those of the uncoated mirror from 700 to 2500 nm, resulting in similar or higher overall average solar specular reflectance measured on the uncoated mirror. The difference in the reflectance distribution between the SPH coating (0.937 ± 0.002, $n = 6$) and the uncoated mirror (0.940 ± 0.002, $n = 6$) was negligible [Fig. 2c].

3.2. Adhesive force reduction of the SPH coating

The NP-textured coating significantly reduced the adhesive force of dust particles on the surface. The adhesion force between a particle and a substrate can be expressed in terms of van der Waals (vdW), electrostatic, and capillary forces.[27–31] The

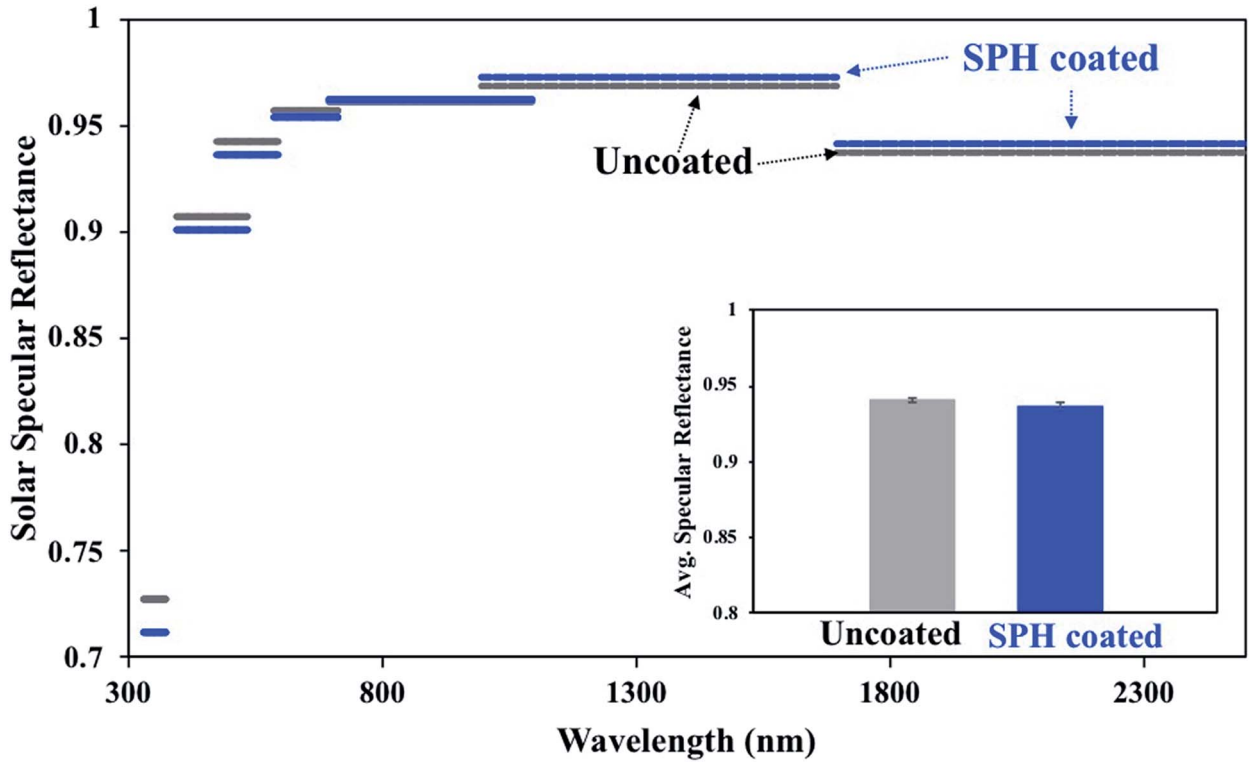

Fig. 2 Solar specular reflectance measured in wavelength bands across the solar spectrum for SPH-coated and uncoated mirrors. Inset is average specular reflectance of an SPH surface and an uncoated mirror surface (7.6 × 7.6 cm^2, $n = 6$). Error bars are the standard deviations in the mean values.

contribution of the capillary force can be significant when water is present between the interacting surfaces as a result of water condensation on the surface of the coating. The SP and SPH coatings were tested in a dry environment. Therefore, water condensation and capillary forces were not considered in this study. The electrostatic force between the particle and the surface is also dependent on the environmental conditions and was not considered. In the present study, we focused on fine particles (*i.e.*, airborne dust) with diameters less than 70 μm.[13] When the particle size is less than 50 μm, the primary adhesion force of the particle is the vdW force.[25] Excluding the electrostatic interactions, the adhesion force between dry sand particles and a glass surface is predominantly vdW force. Several models have been developed to predict and understand the adhesion force between a spherical particle and a nanostructured surface.[21,31,33–36] We developed the adhesion force prediction based on the vdW force (F_{vdW}) between a particle and a surface asperity and expressed the F_{vdW} as a function of the root mean square (RMS) surface roughness value and the distance between the surface asperities.[21,33]

$$F_{vdW} = \frac{AD}{12a^2}\left[\frac{1}{1+\left(\frac{16Dk_1\mathrm{rms}}{\lambda^2}\right)}+\frac{1}{1+\left(\frac{k_1\mathrm{rms}}{a}\right)^2}\right] \quad (1)$$

In eqn (1), A is the Hamaker constant, D is the particle diameter (15 μm), a is the distance between the particle and the surface (~0.3 nm, when the particle is in contact with the surface), rms is the RMS surface roughness, k_1 is a constant (1.817), and λ is the distance between the asperities. The Hamaker constant was calculated according to the mixing rule for dissimilar surfaces $A = \sqrt{A_1A_2}$, where A_1 is the Hamaker constant for the fused silica (6.5×10^{-20} J) and A_2 is the Hamaker constant for the substrate (*e.g.*, polytetrafluoroethylene [3.8×10^{-20} J] for the SP surface, silica for the SPH surface).[27]

Fig. 3a shows that the vdW attraction (*i.e.*, adhesion force) between the SP/SPH surfaces and a model particle (15 μm diameter) decreases when the surface roughness increases. The calculated adhesion force on the SPH coating is ~30% higher than the force on the SP coating. Interestingly, the experimentally measured adhesive force on the SPH coating was ~4.1 times smaller than the adhesive force on the uncoated substrate and slightly lower than on the SP coating. Note that the good agreement between the measured and predicted values indicates the adhesion force between the dust particles and the coated substrates is dependent on the surface roughness, regardless of the surface functionalities. This behaviour agreed well with the modelling results.[21] Fig. 3b–d show the AFM surface morphology analysis of the coated substrates. The bare SiO_2 NP layer of the SPH coating had a uniform surface texture with 25.1 nm of RMS roughness at 2.5 × 2.5 μm^2, whereas the flurosilane molecule coating on the SP surface slightly smoothened the surface texture, giving it 21.6 nm of RMS

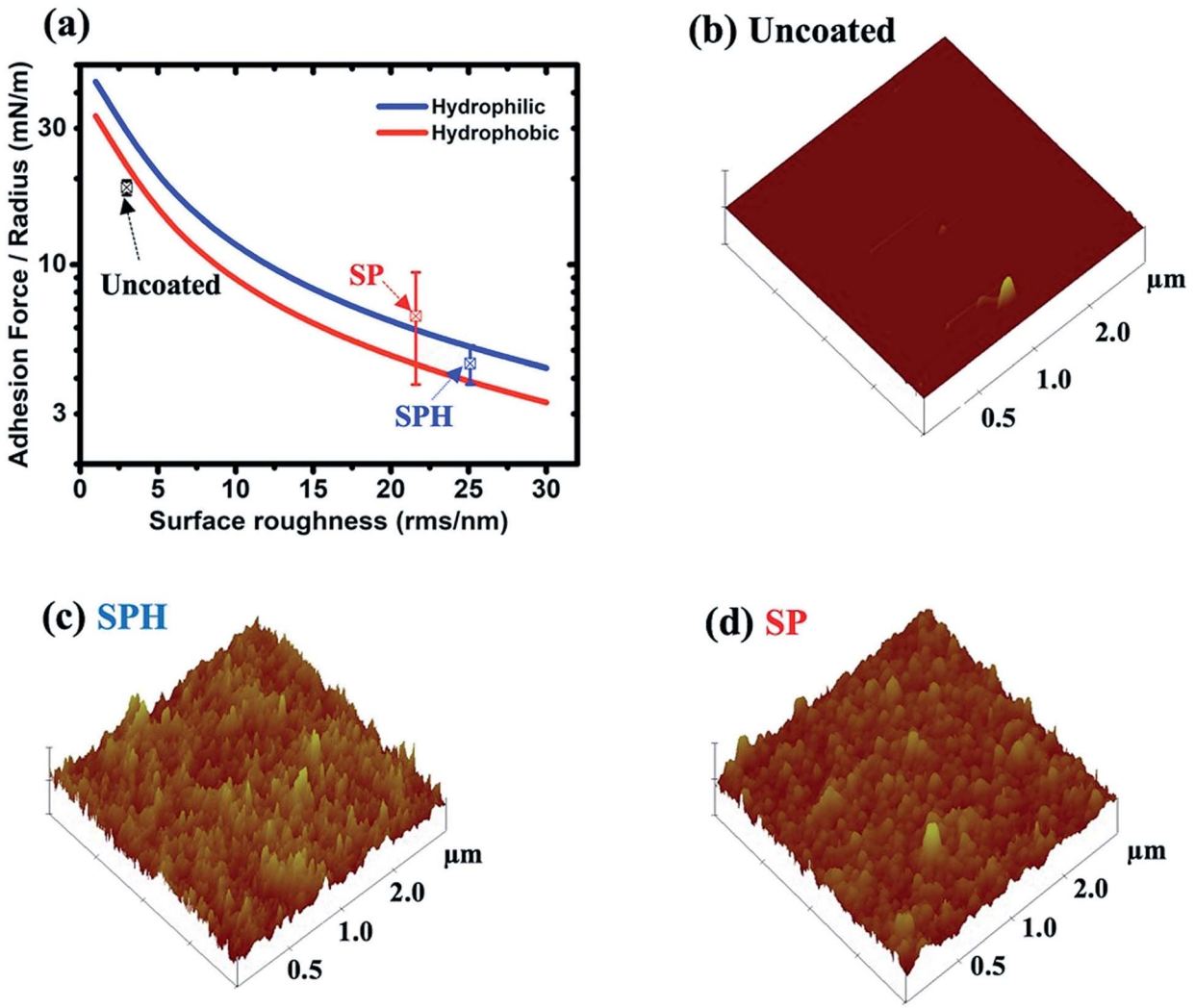

Fig. 3 (a) Measured and calculated adhesion force between a silica sphere (15 μm diameter) and SP and SPH surfaces. AFM surface morphology analysis of (b) uncoated surface (c) SPH coating, and (d) SP coating.

roughness. The uncoated surface (*i.e.*, bare silicon wafer) showed 3.0 nm of RMS roughness.

Fig. 4 shows the adhesive force of a model particle (6 μm) on SPH-coated, SP-coated, and uncoated mirror surfaces as a function of RH. The adhesive forces on the SPH- and SP-coated mirrors were >2.5 times lower than on the uncoated surface at 2–80% of RH. The adhesive force of the particles on the uncoated mirror surface increased with increasing RH. The behaviours of the SP coating as a function of humidity were well matched with the previous results.[21] The observation that the SPH-coated mirror retained similar adhesive forces as the humidity increased was counterintuitive. Because of strong capillary condensation, the adhesion force between particle and substrate generally increases with an increase in humidity.[29,31] However, the humidity effect is more complicated because of the interaction between electrostatic force and capillary force associated with the surface chemistries of particles and substrates.[29] For example, for hydrophilic surfaces, excessive water adsorption attenuates the surface charge by providing a path for leakage, which might cancel out the electrostatic force, leading to a reduction in the adhesive force.[29]

3.3. Anti-soiling and self-cleaning performance of SPH-coated mirror

The SPH-coated mirrors demonstrated excellent soil repellence and a unique self-cleaning capability with facile water layer sliding. Fig. 5 shows a photographic observation of soiling when 1 g of dust (=220 g m^{-2}) was applied to a mirror, inclined at 45°, with half its area SPH coated and other half uncoated. Mostly large dust particle agglomerates (a few millimetres in size) were sparsely scattered on the SPH-coated surface, and large agglomerates and small particles were densely spread on the uncoated surface [Fig. 5b]. To simulate natural winds and the surface cleaning effect,[13] airbrushing with a bulb dust blower (air volume ≅ 40 ml) was applied to remove the loose dust. The small amount of blowing air effectively removed most of the dust particles on the SPH-coated surface and restored the clean surface. An optical microscopy image shows a few sparse fine

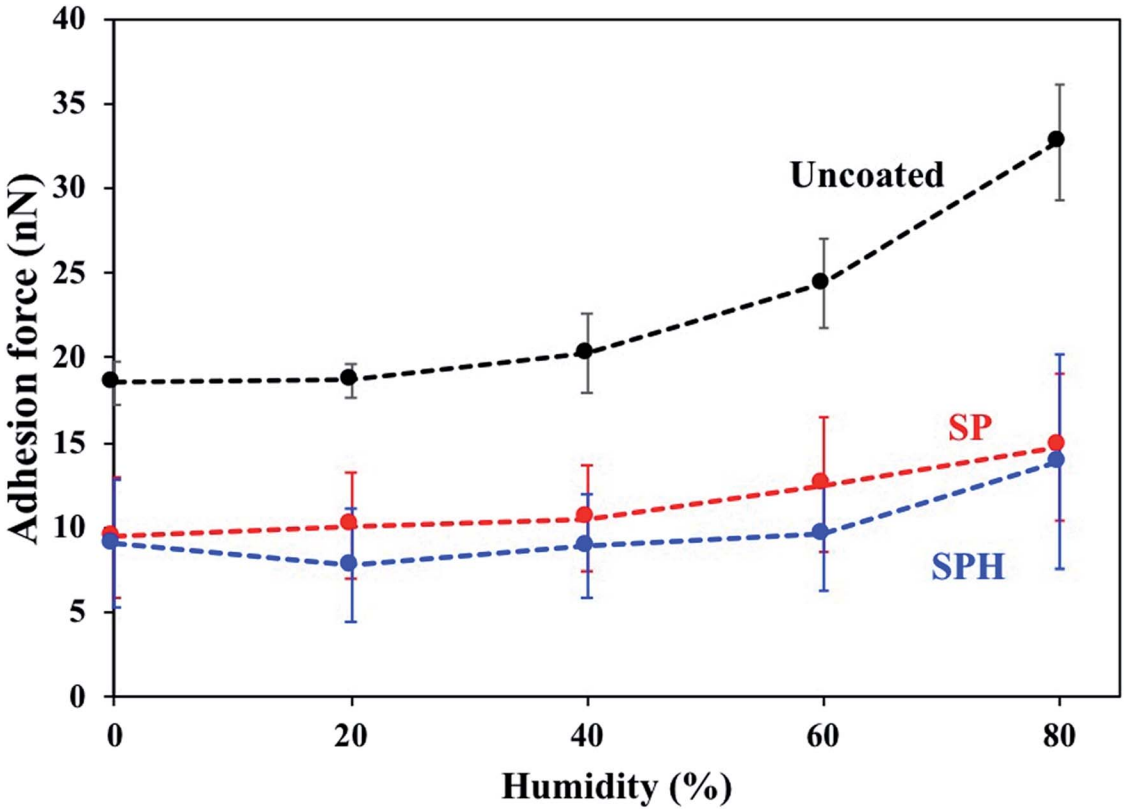

Fig. 4 Adhesive force of spherical dust particles with 6 μm diameters on SPH-coated, SP-coated, and uncoated mirrors as a function of relative humidity.

particles (<5 μm) remaining on the surface [Fig. 5c]. The particle size distribution on the SPH-coated surface was narrow and centred at 1.32 ± 0.62 μm (n = 30 from 8977 μm^2 of image analysis area), which was similar to the soiled-particle size distribution on the SP-coated surface.[21] The standard test soil for the dust soiling has a very broad size range of 0.9–352 μm. Only 12.5 vol% of the test soil had fine particles of <5 μm. The image shows that a very small portion of the fine particles were adhered to the NP-textured surfaces because of the reduction in the adhesion force. However, as reported in the previous work, the small dust particles (~10 μm) were still densely and strongly adsorbed onto the uncoated mirror surfaces as a result of the vdW force, a charge double layer, surface energy, capillary forces, and electrostatic force on the mirror surfaces.[13,14] The particle size distribution on the uncoated surface was broad and centred at 2.03 ± 1.49 μm (n = 375 from 8977 μm^2 of image analysis area). Typically, most soiled dust particles on reflective substrates are <40 μm in dry and desert areas.[7,9] After a few water droplets were deposited on the SPH-coated mirror, unidirectional water layers were observed sliding to the bottom of the mirror edge along the 45° slope of the mirror [Fig. 5d]. The uncoated mirror experienced nonuniform water sliding, which stopped two-thirds of the way from the top edge of the mirror. The facile water sliding results indicated that the SPH-coated mirror demonstrated effective self-cleaning. Fig. 5e shows water-dispersed soil suspensions dropped on clean mirror surfaces. The soil suspended in water easily spread out on the SPH-coated surface, and soil residues were left on the surface after drying. For the uncoated mirror, soiled water droplets formed on the surface and left dense cake-like residues. The soil residues on the SPH-coated surface were not simply rinsed out, because the wet condition added a very large capillary force to the adhesion force between the particles and the surface.[31,32] In humid conditions, the capillary force could be 1 order of magnitude larger than the vdW force.[31] The soil residues were removed by gentle brushing with water, and the coated surface exhibited superhydrophilicity after the brushing.

The AS performance of the SPH-coated mirror was compared with that of the SP-coated and the uncoated mirrors [Fig. 6]. Solar reflectance measurements were carried out with three mirrors inclined at 45° elevations after gravimetric soiling and following airbrushing. The applied soiling amount was increased to the simulated 1 year accumulation expected in the Arizona desert area (*i.e.*, ~909 g m^{-2}).[21,36] Our previous work reported that an SP-coated mirror (called the AS-coated mirror) exhibited excellent AS performance, resulting in no reflectance loss after soiling in an indoor soiling experiment.[21] The uncoated mirror had a reduction in reflectance associated with the soiling rate and elevation. As we reported, the reflectance of the uncoated mirror dramatically decreased with an increasing soiling rate. Note that the solar reflectance of SPH-coated mirrors showed no decrease as soiling rates increased. Both the SP and SPH coatings showed similar outstanding AS performance due to the engineered surface roughness, which

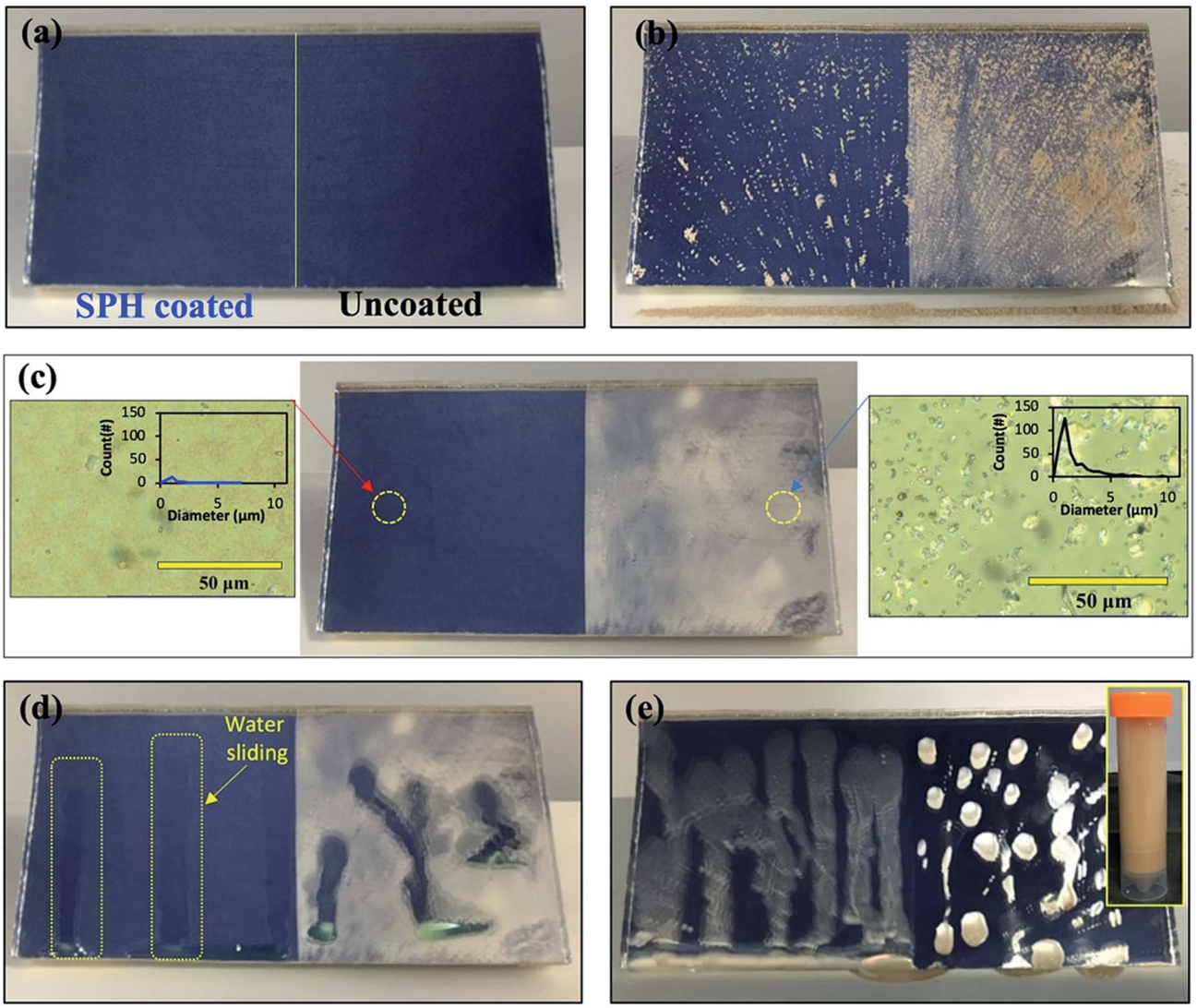

Fig. 5 Observation of soiling on a mirror (15.2 × 7.6 cm^2) with half its area coated with nanoparticles to give it SPH properties. (a) A half-coated mirror at 45° elevation, (b) initial soiling (1 g) on the mirror, (c) dust accumulation on the mirror surface after airbrushing. Insets are optical microscope (5000× magnification) images of soiling on an SPH-coated mirror and an uncoated mirror after airbrushing. (d) Water dripping on the mirror surfaces. The water was coloured with a green dye. (e) Water disperses soil dripping on the mirror surfaces. Inset is the suspended soil that was collected from the suspension in 0.1 g ml^{-1} of soil and water mixture (ISO 12103-1 A4 Coarse Sand).

was associated with an adhesion force reduction. This finding suggests that the engineered surface roughness is a key factor in AS performance, regardless of the surface functionality.

3.4. Field evaluation of comparative SPH- and SP-coated mirrors

A field examination of environmental soiling on SPH-coated, SP-coated, and uncoated mirrors (15.0 × 20.0 cm^2 in size) was carried out for 234 days on a sloping roof (45° elevation) at Oak Ridge National Laboratory during the late fall, winter, spring, and summer seasons. The soiling conditions in Oak Ridge, Tennessee, USA (*e.g.*, high humidity, high concentrations of pollen and organic aerosols produced by the surrounding forest, frequent rain) are much different from those in the dry or semi-arid desert environments where CSP plants are sited. Some reduction in daily soiling was alleviated by natural cleaning provided by rain, heavy morning dew, snow, and frost formation during the field test period.

Specular reflectance measurements across the full solar spectrum showed that the daily degradation of reflectance (DDR) on the SPH-coated mirror was quantitatively lower than the DDR of the uncoated mirror [Fig. 7]. Both SPH- and SP-coated mirrors showed a similar higher retention of reflectance, compared with the uncoated mirror, over 79 days. The SP- and SPH-coated mirrors exhibited their unique self-cleaning capability after rain events. (Photographs of mirror statuses 1, 2, and 3 in Fig. 7a are available in the ESI.‡) Our previous work showed the SP-coated mirror maintained a lower DDR than the uncoated mirror for 61 days during the late summer and the early fall seasons.[21] However, over long-term exposure, the SP-

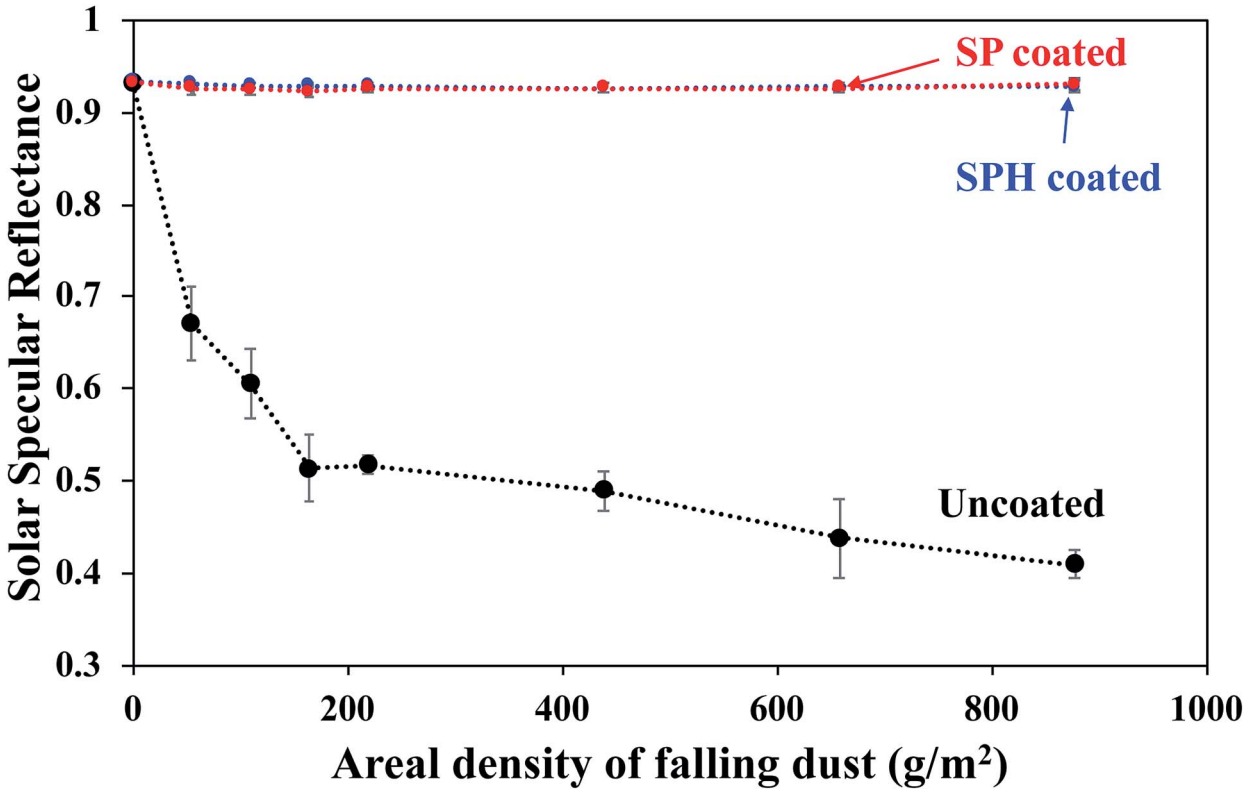

Fig. 6 Solar specular reflectance analysis of dusting effects on SPH-coated, SP-coated, and uncoated mirrors as an increasing amount of dust was applied to the mirrors at elevations of 45° after airbrushing. The number of measurements per data point was ≥5, and the error bars are the standard deviations in mean values. Lines are drawn for illustration.

coated mirror experienced a distinguishable decrease in reflectance, with a significant loss of dewetting performance, after 99 days. (Photographs of mirrors at status 4 in Fig. 7a are available in the ESI.‡). The entire SP-coated mirror surface showed hard water marks, and rainwater droplets formed on the entire mirror surface after light rain events. It appears that the distinguishable DDR of the SP-coated mirror, induced by hard water marking, was associated with the beginning of the pollen season (*e.g.*, late February). After that time, the DDR of the SP-coated mirror was similar to the DDR of the uncoated mirror.

Note that the reflectance of the SPH-coated mirror was 2 to 7% greater than that of the SP-coated and the uncoated mirrors over a period of 220 days. Also, the standard deviation in the average value of the reflectance of the SPH-coated mirror was significantly smaller than the deviation in the average reflectance of the other mirrors. After 160 days, all mirrors experienced a distinguishable reduction in reflectance (*i.e.*, ~4% for SPH-coated and ~8% for SP-coated and uncoated mirrors) because of the high concentration of organic foulants (*e.g.,* airborne pollen particles) and low precipitation amounts in the late spring. (Photographs of the mirrors at status 6 in Fig. 7a are available in the ESI.‡) After 160 days, the reflectance of the SP-coated mirror was not restored by natural cleaning, whereas the reflectance of the uncoated mirror recovered slightly after frequent rains. It appears the hydrophilic surface (which induced fast water layer sliding) had better self-cleaning performance associated with weathering than the hydrophobic surface (which induced water droplet rolling).

Our previous study reported that a possible dust fouling mechanism manifested as a loss in reflectance could be induced by a dust-moisture cementation process.[21] Atmospheric dust contains a distribution of inorganic and organic particulates (*e.g.*, pollen) that contain some water-soluble and insoluble salts. At high humidity, water-soluble dust particles on the surface form microscopic droplets of salt solutions that also retain any insoluble particles. When dried, the precipitated salt acts as a cement to anchor insoluble particles to the surface. Another possible dust-cementation mechanism of the SP-coated mirror in this field area could be airborne dust absorption on microscopic water droplets on mirror surfaces under humid and wet conditions. Generally, an SP-coated surface has bulk water repellence, but microscopic water droplets can form between NPs, on possible defects due to the SP-coated surface, and on direct fouling from the field area (*e.g.,* bird droppings, fouling from the portable reflectometer measurement). Airborne organics (*i.e.*, pollen and its fibres) were adsorbed on the microscopic droplets, and microorganic fouling accumulated over time [see ESI‡]. It appears that the hydrophilic self-cleaning mechanism may be more effective in mitigating dust cementation and airborne organic adsorption than the hydrophobic self-cleaning mechanism. The cemented organic dust aggregations and water marks were not rinsed away until mechanical brushing was used.

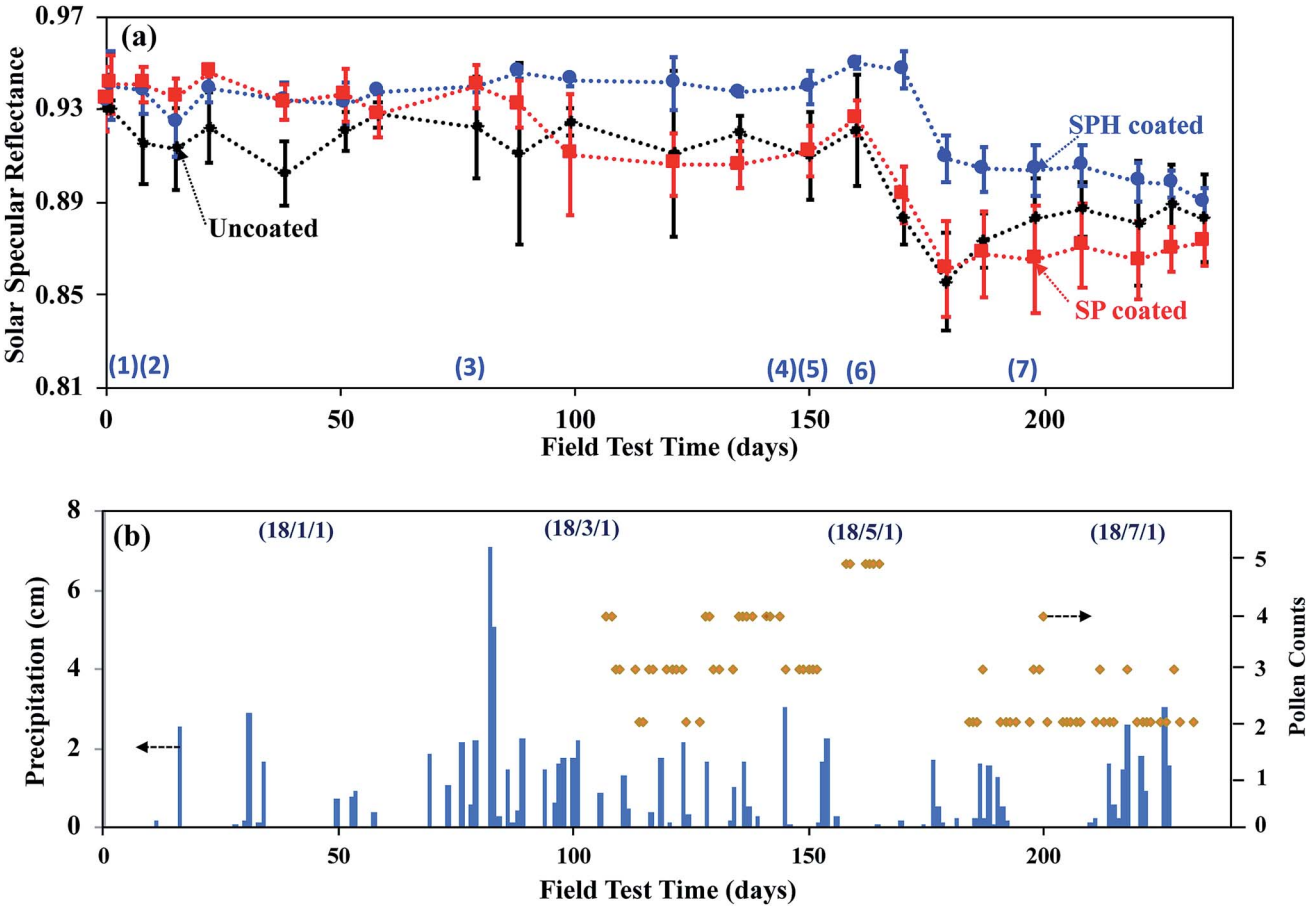

Fig. 7 (a) Solar specular reflectances of SPH-coated, SP-coated, and uncoated mirrors measured during 234 days of outdoor exposure. Photographic images of each mirror status, designated by number, are available in the ESI.‡ The number of measurements per data point was ≥6, and the error bars are the standard deviations in mean values. Lines are drawn for illustration. (b) Corresponding weather conditions in Oak Ridge, Tennessee, USA. Blue bars and orange lines indicate the precipitation levels and airborne pollen counts (from www.weather.com) during the field test period. The maximum pollen count was 5 grains per m^3 during the test period. Some data points for air pollen counts in the figure were not reported.

Fig. 8 shows the characteristics of the three weathered mirrors after 234 days of outdoor exposure. The samples were cut to 7.6 × 7.6 cm^2 for further characterization. The SPH-coated mirror still exhibited an average WCA of 7.2 ± 2.3° (n = 6), slightly increased from the average WCA of 4.8 ± 3.5° (n = 10) at 0 day. The SP-coated mirror exhibited an average WCA of 111.0 ± 3.9° (n = 6), significantly decreased from an average WCA of 164.9 ± 0.9° (n = 10) at 0 day. The change in WCA was associated with organic dust accumulation on the mirror surfaces [Fig. 9 and ESI‡]. Fig. 9 shows an SEM image of the weathered SPH-coated and SP-coated mirrors. The NP coatings on the weathered SPH-coated and SP-coated mirrors were present, providing the surface roughness for hydrophilicity and hydrophobicity, respectively. The uncoated mirror had an average WCA of 42.7 ± 1.9° (n = 6), a decrease from the average WCA of 52.6 ± 19.0° (n = 30). Then 1 g soiling followed by airbrushing was carried out on the weathered mirrors to evaluate the AS performance. Note that the weathered SPH- and SP-coated mirrors still showed no adhesion of soiling dust particles, corresponding to no decrease in solar reflectance, whereas the weathered uncoated mirror exhibited a large reflectance reduction with soiling [Fig. 10]. This is a significant result for the design of AS-coated mirrors for CSP mirror applications in arid areas.

Another outdoor weathering test was performed on mirrors with various WCAs during a 1 day interval in the field area. The topography and surface functionality of the coatings were controlled by varying the sol–gel/NP weight ratio from 4 to 64. First, drawdown coating was conducted on a 20 × 30 cm^2 second-surface solar mirror. Half of the coated mirror was cut to fabricate a mirror with a hydrophobic coating. For the as-is mirrors (*i.e.*, hydrophilic, H-1, 2, 3, and 4), as the sol–gel/NP ratio increased, the WCA increased from 4.8° to 57.5°. For the post-functionalized mirrors (hydrophobic, P-1, 2, 3, and 4), as the sol–gel/NP ratio increased, the WCA decreased from 164.9° to 111.2°. The H-series and P-series mirrors had different surface functionalities based on the same surface morphology structure. Fig. 11 shows that the mirrors with hydrophilic behaviour outperformed the mirrors with hydrophobic behaviour in maintaining clean surfaces. For mirrors with hydrophobic surfaces, the reflection reduction of the P-1 mirror, assigned to the SP-coated mirror, was less than that of the other

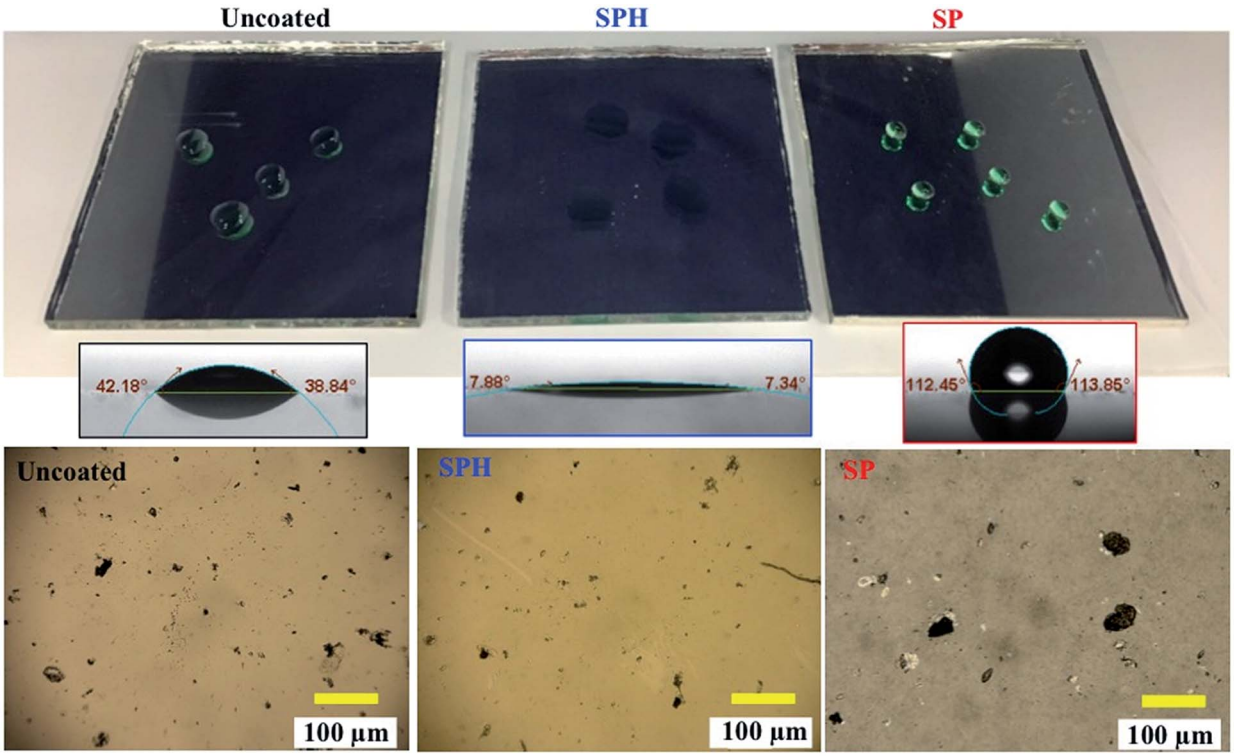

Fig. 8 Surface characteristics and optical microscopic images (500× magnification) of SPH-coated, SP-coated, and uncoated mirrors after 234 days of outdoor exposure. Insets are the water contact angle measurements on the mirrors (the measured water droplet volume = 5–10 μl).

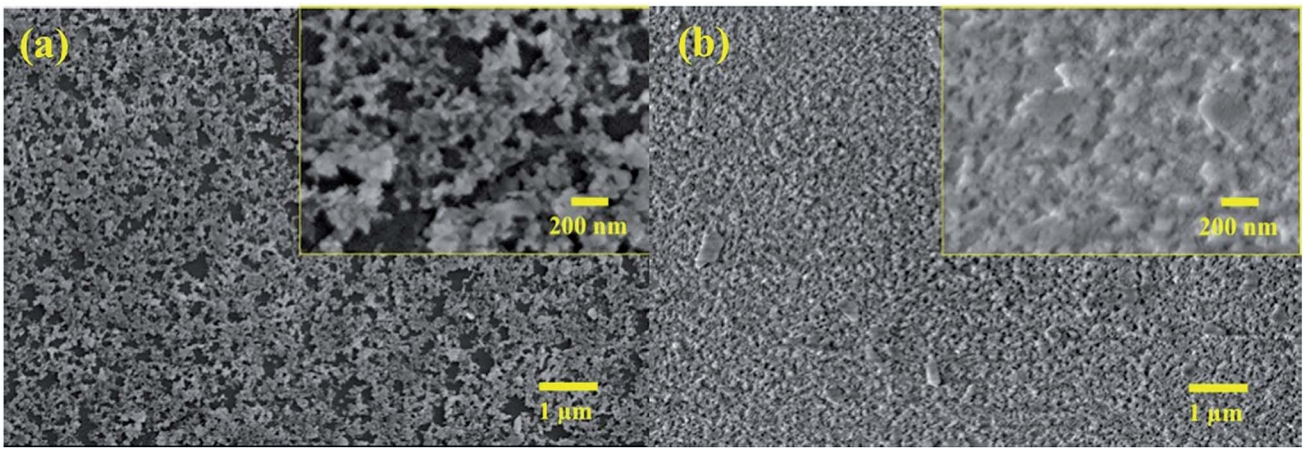

Fig. 9 SEM image of (a) SPH-coated and (b) SP-coated mirror after a 234 day outdoor field test.

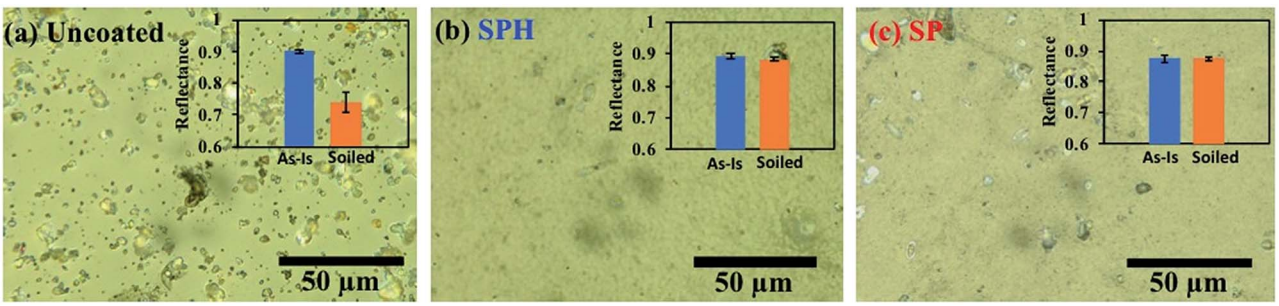

Fig. 10 Optical microscope images of soiling (1 g) after 234 days of weathering of SP-coated, SPH-coated, and uncoated mirrors after air-brushing. (a) Uncoated mirror surface at 5000× magnification, (b) SPH-coated mirror surface at 5000× magnification, (c) SP-coated mirror surface at 5000× magnification.

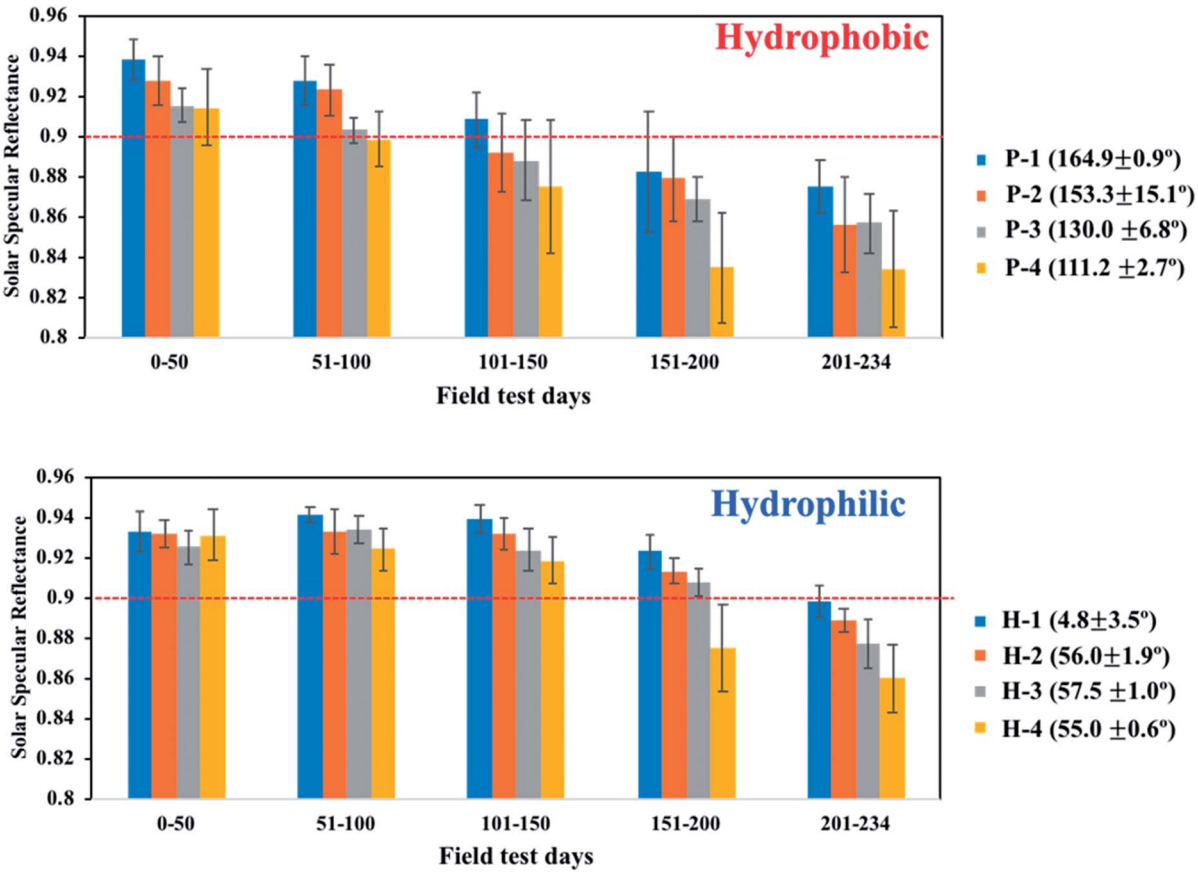

Fig. 11 Solar specular reflectance analysis of outdoor dusting effects on various mirrors from 5 to 165° WCA. Mirrors were exposed for 234 days in Oak Ridge. The one bar result is the average reflectance over the period. The number of measurements per data point was ≥30. Error bars are standard deviations in mean values of reflectance. The red dotted line indicates 0.9 of reflectance.

hydrophobic mirrors; whereas the H-1 mirror, assigned to the SPH-coated mirror, exhibited the lowest reflectance reduction among the hydrophilic mirrors. All SPH-coated mirrors maintained their unique surface morphology after the field test [ESI‡]. Therefore, we carefully suggest that the SPH coating had better AS performance than the SP-coated mirror in the humid valley area around Oak Ridge.

4. Conclusions

Facile and environmentally friendly silica oxide NP-textured coatings revealed excellent AS and unique self-cleaning performance associated with superhydrophilicity. The engineered surface roughness associated with superwetting significantly decreased the adhesive force of dust particles on a mirror surface, resulting in an intrinsic repellence of inorganic soil and dust particles and enhancement of self-cleaning behaviour due to facile water layer sliding. Compared with the AS performance of SP coatings, the SPH coating exhibited an ~2.5 × enhancement of AS performance in outdoor field testing. Superhydrophilicity was more effective in reducing organic dust-cementation soiling on the mirror surface. Considering the fabrication process, cost, and extra energy-intensive cleaning cycles, SPH NP-textured coatings are expected to result in highly efficient solar energy harvesting.

Conflicts of interest

There are no conflicts to declare.

Acknowledgements

This research was conducted at Oak Ridge National Laboratory (ORNL), which is managed by UT Battelle, LLC, for the US Department of Energy (DOE) under contract DE-AC05-00OR22725. The work was sponsored by the Solar Energy Technologies Office within the DOE Office of Energy Efficiency and Renewable Energy. Some of the materials characterization (including SEM and AFM humidity measurement) was conducted at the Center for Nanophase Materials Sciences, which is sponsored by the ORNL Scientific User Facilities Division and the DOE Office of Basic Research Sciences.

References

1 S. Bouaddi, A. Ihlal and A. Fernandez-García, *Renewable Energy*, 2017, **101**, 437–449.
2 M. R. Maghami, H. Hizam, C. Gomes, M. A. Radzi, M. I. Rezadad and S. Hajighorbani, *Renewable Sustainable Energy Rev.*, 2016, **59**, 1307–1316.
3 M. Abderrezek and M. Fathi, *Sol. Energy*, 2017, **142**, 308–320.

4 M. Saidan, A. G. Albaali, E. Alasis and J. K. Kaldellis, *Renewable Energy*, 2016, **92**, 499–505.
5 M. J. Adinoyi and S. A. M. Said, *Renewable Energy*, 2013, **60**, 633–636.
6 Q. Xu, Z. Zhao, X. Zhu, L. Cheng, S. Bai, Z. Wang, L. Meng and Y. Qin, *Nanoscale*, 2016, **8**, 17747.
7 T. Sarver, A. Al-Qaraghuli and L. L. Kazmerski, *Renewable Sustainable Energy Rev.*, 2013, **22**, 698–733.
8 A. Sayyah, M. N. Horenstein and M. K. Mazumder, *Sol. Energy*, 2014, **107**, 576–604.
9 W. Javed, Y. Wubulikasimu, B. Figgis and B. Guo, *Sol. Energy*, 2017, **142**, 123–135.
10 B. Figgis, A. Ennaoui, S. Ahzi and Y. Remond, *Renewable Sustainable Energy Rev.*, 2017, **76**, 872–881.
11 H. Lu and W. Zhao, *Appl. Energy*, 2018, **220**, 514–526.
12 A. A. Merrouni, F. Wolfertstetter, A. Mezrhab, S. Wilbert and R. Pitz-Paal, *Energy Procedia*, 2015, **69**, 1948–1957.
13 G. Picotti, P. Borghesani, M. E. Cholette and G. Manzolini, *Renewable Sustainable Energy Rev.*, 2018, **81**, 2343–2357.
14 G. Picotti, P. Borghesani, G. Manzolini, M. E. Cholette and R. Wang, *Sol. Energy*, 2018, **173**, 1287–1305.
15 Y. Si and Z. Guo, *Nanoscale*, 2015, **7**, 5922.
16 J. T. Simpson, S. R. Hunter and T. Aytug, *Rep. Prog. Phys.*, 2015, **78**, 086501.
17 Y. Li, Z. Zhang, M. Wang, X. Men and Q. Xue, *J. Mater. Chem. A*, 2017, **5**, 20277–20288.
18 J. E. Mates, R. Ibrahim, A. Vera, S. Guggenheim, J. Qin, D. Calewarts, D. E. Waldroup and C. M. Megaridis, *Green Chem.*, 2016, **18**, 2185–2192.
19 A. Rifai, N. Abu-Dheir, M. Khaled, N. Al-Aqeeli and B. S. Yilbas, *Sol. Energy Mater. Sol. Cells*, 2017, **171**, 8–15.
20 V. A. Ganesh, H. K. Raut, A. S. Nair and S. Ramakrishna, *J. Mater. Chem.*, 2011, **21**, 16304–16322.
21 G. G. Jang, D. B. Smith, F. A. List III, D. F. Lee, A. V. Levlev, L. Collins, J. Park and G. Polizos, *Nanoscale*, 2018, **10**, 14600.
22 G. Polizos, J. K. Sharma, D. B. Smith, E. Tuncer, J. Park, D. Voylov, A. P. Sokolov, H. M. Meyer and M. Aman, *Sol. Energy Mater. Sol. Cells*, 2018, **188**, 255–262.
23 J. Drelich and E. Chibowski, *Langmuir*, 2010, **26**(24), 18621–18623.
24 T. Lorenz, E. Klimm and K.-A. Weiss, *Energy Procedia*, 2014, **48**, 749–756.
25 M. Peng, J. Qi, Z. Zhou, Z. Liao, Z. Zhu and H. Guo, *Langmuir*, 2010, **26**(16), 13062–13064.
26 L. Li, B. Li, J. Dong and J. Zhang, *J. Mater. Chem. A*, 2016, **4**, 13677–13725.
27 J. N. Israelachvili, *Intermolecular and Surface Forces*, Academic Press, London, 3rd edn, 2011.
28 X. Xiao and L. Qian, *Langmuir*, 2000, **16**, 8153–8158.
29 H. Kweon, S. Yiacoumi and C. Tsouris, *Colloids Surf. A*, 2015, **481**, 583–590.
30 H. Kweon, S. Yiacoumi and C. Tsouris, *Langmuir*, 2011, **27**, 14975–14981.
31 S. You and M. P. Wan, *Langmuir*, 2013, **29**, 9104–9117.
32 R. A. A. Bowling, in *Particles on Surfaces 1, Theoretical Review of Particle Adhesion*, ed. K. L. Mittal, Springer, Boston, MA, 1988.
33 Y. I. Rabinovich, J. J. Adler, A. Ata, R. K. Singh and B. M. Moudgil, *J. Colloid Interface Sci.*, 2000, **232**, 10–16.
34 W. Cheng, P. F. Dunn and R. M. Brach, *J. Adhes.*, 2002, **78**, 929–965.
35 M. Gotzinger and W. Peukert, *Langmuir*, 2004, **78**, 5298–5303.
36 G. Polizos, G. G. Jang, D. B. Smith, F. A. List, M. G. Lassiter, J. Park and P. G. Datskos, *Sol. Energy Mater. Sol. Cells*, 2017, **176**, 405–410.